A multi-scale approach for performance assessment of hydrogenated graphene Field-Effect Transistors

G. Fiori, S. Lebègue,* A.Betti, P. Michetti†, M. Klintenberg‡, O. Eriksson‡, G. Iannaccone
Dipartimento di Ingegneria dell'Informazione, Università di Pisa, Via Caruso 16, 56122 Pisa, Italy
* Institut Jean Barriol, Nancy Université BP 239, 54506 Vandoeuvre-lès-Nancy, France
†Institute for Theoretical Physics and Astrophysics, D-97074 Wuerzburg, Germany
‡Department of Physics and Astronomy, Uppsala University, Box 516, SE-75120, Uppsala, Sweden

***Abstract*—Performance analysis of Field Effect Transistors based on hydrogenated graphene is performed through a multi-scale approach based on calculations of the energy bands by means of GW approximation, a three-nearest neighbor (3NN) sp^3 tight-binding Hamiltonian, and a ballistic transport model. The considered device exhibits large I_{on} and I_{on}/I_{off} ratios, due to the large bandgap, with reduced lithographic constrains as compared to one-dimensional channels.**

I. Introduction

Chemical functionalization has very recently demonstrated to represent a viable solution in band gap engineering of graphene-based materials [1].

Real performance and application perspectives of graphene still have to be addressed, due to the embryonic stage of the fabrication process, so that theoretical simulations can provide important information concerning the performance assessment.

Simulations aiming at predicting electronic behavior of devices based on such a new material need to take into account all the relevant physical effects playing at the atomic scale.

Sofo et al. [4] first predicted stability of 100% hydrogenated graphene through standard DFT calculations with a Generalized Gradient Approximation (GGA). More detailed simulations have been performed in [5], where DFT deficiencies in calculating energy gap have been overcome through GW simulations, showing energy gaps of 5.4 eV and 4.9 eV for the chair and the boat conformation, respectively, thus correcting results in [4] and [6] by almost 2 eV. Non-ideal structures have been studied in [7], through geometry optimization and molecular dynamics simulations.

As can be seen, ab-initio simulations are the method of choice in order to accurately model the band structure, but they are too computationally demanding when a complete transistor consisting of thousands of atoms needs to be investigated.

In this work we present, for the first time, the performance analysis of Field Effect Transistors based on recently fabricated 100% hydrogenated graphene [1] (the so-called graphane) and theoretically predicted semi-hydrogenated graphene (i.e. graphone) [2]. The computational strategy is based on a multi-scale approach based on accurate GW calculations of the energy dispersion relations, and a fitting of the computed energy bands by means of a three-nearest neighbor sp^3 tight-binding Hamiltonian to be included in a semiclassical model, based on the assumption of ballistic transport.

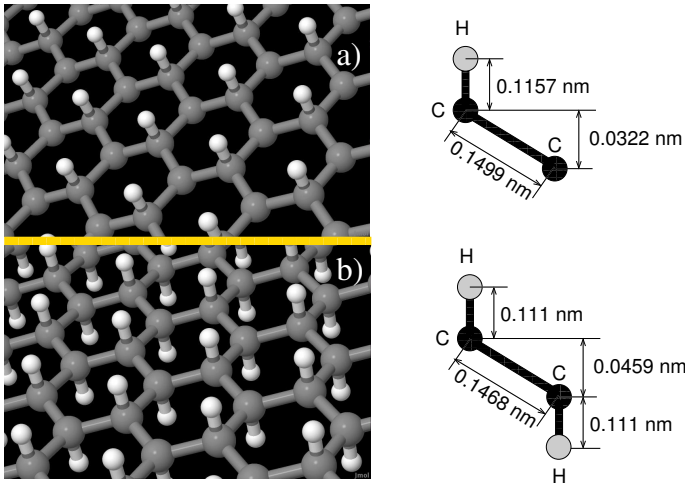

Fig. 1. Lattice of the a) half-hydrogenated and b) full hydrogenated graphene, and lateral views.

A. Results and discussion

In Figs. 1a-b, we show the lattices of full and semi-hydrogenated graphene, whose atoms positions have been computed by means of GW simulations: atoms displacements, as well as the atom-atom distances are shown on the right. As can be seen, C atoms belonging to graphane and graphone lattice are not in-plane as in graphene, and the C-C distance (0.142 nm in graphene) are equal to 0.1468 nm and 0.1499 nm, respectively. C-H distance instead is 0.1157 nm for graphone and 0.111 nm for graphene, in agreement with previous DFT calculations [4].

The energy bands computed by means of three different models are shown in Fig. 2: three-nearest neighbor sp^3 tight-binding Hamiltonian (solid line), DFT within generalized gradient approximation (GGA) (dashed line) and GW (dots) [8], [9]. DFT and GW calculations have been performed by means of the Vienna Ab-initio Simulation Package [10], [11].

In order to help convergence of GW simulations, we have considered 200 bands for the corresponding summation in the calculation of the polarizability and the self-energy, while we have used a cut-off of 150 eV for the size of the polarizability matrices.

978-1-4244-9382-1/10/$26.00 ©2010 IEEE

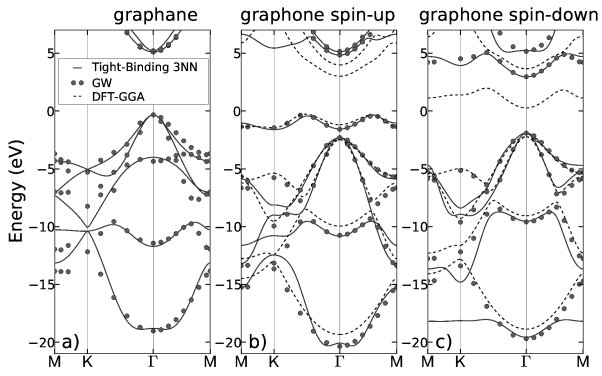

Fig. 2. Energy bands computed for graphane (a) and graphone (b-c), using tight-binding three-nearest neighbor (solid line), GW (dots) and DFT-GGA approaches (dashed lines). In the case of graphone spin-up (b) and spin-down bands (c) are shown.

In the chair conformation, which is the most stable [4], the gap in graphane is direct and in correspondence of the Γ point, and the bandgap is equal to 3.5 eV for the GGA, and 5.4 eV [5] for the more precise GW approximation. In the same way, the transitions at the high-symmetry points M and K are increased when considering GW: from 10.8 eV to 13.7 eV at the M point, and from 12.2 to 15.9 eV at the K point [5]. The GW bandstructure of graphane presented here is exactly equivalent to the one in [5], and it is used here as a support for the tight-binding fitting.

In Figs. 2b and 2c, we show spin-up and spin-down energy bands computed by means of the three above-mentioned models for the 50% functionalized graphene sheet (graphone). The valence band maximum is located along the $\Gamma - K$ high-symmetry line (Fig. 2b), and almost degenerate with the other maximum along the $\Gamma - M$ direction. The conduction band minimum is instead at the Γ point (Fig. 2c). For both GW and GGA the gap is indirect. However, while GGA provides a bandgap equal to 0.46 eV, the GW provides a bandgap equal to 3.2 eV. In addition to increasing the band gap, the GW is also modifying the dispersion relation with respect to GGA.

In order to solve the electrostatic and the transport problems in functionalized graphene devices, we have adopted a semiclassical model similar to that in [3], able to compute the free charge density and the current, given the energy bands in the whole Brillouin Zone (BZ). Semiclassical models, although not refined as full numerical simulations, offer easily accessible results, with the possibility to rapidly estimate the performance of a device and identifying possible issues. Schottky tunneling contacts and inelastic relaxation could also be included in semi-analytical models [13] for better accuracy. However, the model here adopted relies on the assumption of fully ballistic transport, since our aim in the current work is to assess the upper limits of device performance. This means that forward-going and backward-going states will be characterized by a steady-state distribution in thermal equilibrium with source and drain, respectively. Two main approximations are also made, typical in Landauer-Buttiker transport models: top-of-the-band approximation and the assumption of long-channel. The first assumption implies that thermionic currents, which flow in the FET channel above the conduction band (or below the valence band maximum), represent the major contribution to transport. We therefore neglect the presence of tunneling currents (both intra and inter-band), which is adequate in a sufficiently long channel device with Ohmic contacts, and for materials with very large bandgap. Long channel ensures full gate control over the electrostatic potential at the center of the channel, avoiding short-channel effects, where capacitive coupling with source and drain becomes important, degrading performance.

The channel current per unit width is given by

$$I = \frac{q}{4\pi^2} \sum_{\pm} \int_{BZ} d\vec{k} v_x \left[f(E^{(x_c)}_{\vec{k},\pm} - \mu_S) - f(E^{(x_c)}_{\vec{k},\pm} - \mu_D) \right], \quad (1)$$

where the integration runs over the Brillouin zone for conduction and valence bands $E^{(x_c)}_{\vec{k},\pm}$, calculated at the center of the channel (at $x = x_c$), where a rigid shift of $-q\Phi_c$ is accounted accordingly to the channel potential Φ_c. f is the Fermi-Dirac distribution function, v_x is the component of the group velocity along the channel.

From a numerical point of view, a large number of k points in the BZ (almost equal to 10^5) is required in order to obtain accurate results, which can be really prohibitive for the GW approach. In order to avoid this problem, the energy dispersion along the ΓM and ΓK directions obtained by the GW approximation, has been fitted by means of a least-mean square procedure and a three-nearest neighbor sp^3 tight-binding Hamiltonian, which provides more accurate fitting than a simple nearest-neighbor approach.

Results are shown in Fig. 2. Particular attention has been paid to the minima and the maxima of the conduction and valence bands, respectively, since such states are those mainly contributing to transport. As can be seen, tight-binding results are in good agreement with GW calculations.

In Fig. 3, we show the structure of the simulated double gate device. The channel is infinitely long and wide and embedded in SiO_2 (ε_r=3.9), which we consider as a representative gate dielectric. Results can be translated to device with different gate dielectrics as long as the capacitance per unit area is the same. In the inset of Fig. 3, we show the device transversal cross-section: $t_{\rm ox1}$ and $t_{\rm ox2}$ are the top and bottom gate oxide thicknesses, respectively.

In order to compute the channel potential ϕ_c, we need to self-consistently solve the vertical electrostatics at the center of the channel (x_c). The following equations, describing the charge density from the point of view of electrostatics and injection statistics, have to be simultaneously solved in order to determine the channel potential Φ_c

$$\begin{aligned} Q &= -C_{G1}(V_{G1} - \Delta_{G1} - \phi_c) - C_{G2}(V_{G2} - \Delta_{G2} - \phi_c) \\ Q &= Q_h + Q_e, \end{aligned} \quad (2)$$

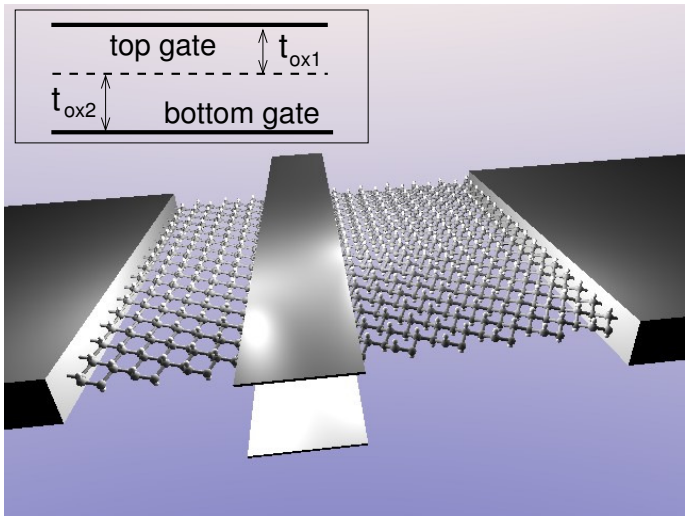

Fig. 3. Sketch of the simulated device. The channel here shown is graphane, but the very same structure has been considered for graphone based FET. In the inset, the device transversal cross-section is shown.

where $C_G = \epsilon_{ox1(2)}/t_{ox1(2)}$ is the top (bottom) gate capacitance per unit area, whereas $\Delta_{G1(2)}$ is the flat band voltages of the top (bottom) gate (set here to 0 V), $V_{G1(2)}$ is the top (back) gate potential with respect to the source contact. The first equation describes the electrostatic charge in the channel due to the capacitive couplings between the gates and the channel itself. The second equation gives a statistical description of the charge density in the channel, due to holes and electrons (Q_h and Q_e), by summing over their steady-state distribution in conduction and valence bands

$$Q_e = -\frac{q}{4\pi^2}\int_{BZ} d\vec{k}[f(E^{(x_c)}_{\vec{k},+} - \mu_S) + f(E^{(x_c)}_{\vec{k},+} - \mu_D)], \quad (3)$$

and valence band

$$Q_h = \frac{q}{4\pi^2}\int_{BZ} d\vec{k}[f(\mu_S - E^{(x_c)}_{\vec{k},-}) + f(\mu_D - E^{(x_c)}_{\vec{k},-})], \quad (4)$$

where forward and backward-moving particles are in equilibrium with source and drain thermal baths, respectively.

In Figs. 4a and 4b, the transfer characteristics of NMOS and PMOS FETs based on graphane and graphone are shown in the linear and logarithmic scale, for $t_{\rm ox1}$=$t_{\rm ox2}$=1 nm, and for a drain-to-source voltage $V_{\rm DS}$=$V_{\rm DD}$=0.8 V. To allow a comparison with the scaling expected for silicon technology, we consider the value of $V_{\rm DD}$ that the International Technology Roadmap for Semiconductors [12] predicts for high performance logic in 2015-2016. Analogously, the current in the OFF state $I_{\rm off}$ has been set to 100 nA/μm.

In the sub-threshold regime, as expected, the sub-threshold swing (SS) is equal to 60 mV/dec, due to the adopted double gate geometry, which assures good gate control over the channel barrier.

As can be seen, all devices are able to provide large currents and present similar transfer characteristics as well as the same

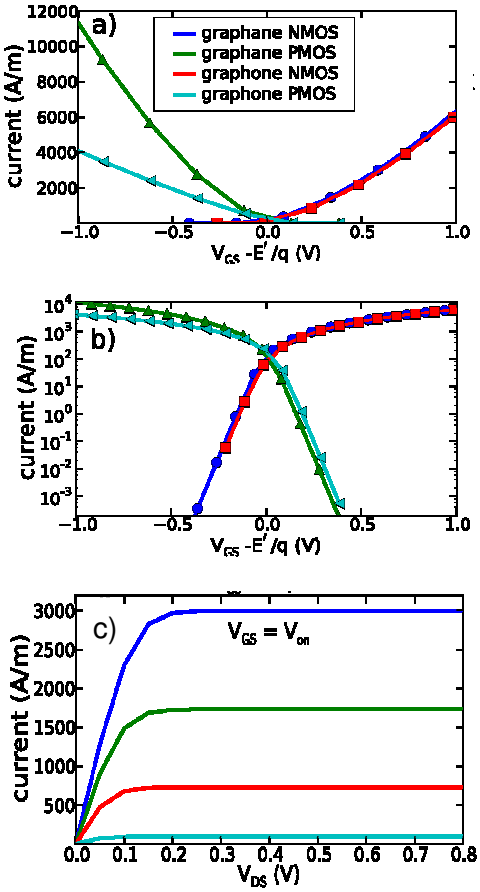

Fig. 4. Transfer characteristics for graphane and graphone NMOS and PMOS in the linear a) and in the logarithmic scale b): each transfer characteristic has been translated by E', the bottom of the conduction band for NMOS and the top of the valence band for PMOS; c) output characteristic for different $V_{\rm GS}$: the gate-to-source step is 0.2 V.

transconductance (derivative of the transfer characteristic with respect to gate-to-source voltage ($V_{\rm GS}$)), except for graphone PMOS, which shows degraded performance.

In Fig. 4c we show the drain-to-source current as a function of $V_{\rm DS}$: the $V_{\rm GS}$ step is equal to 0.2 V.

In Fig. 5, we show the cut-off frequency f_T, the intrinsic delay time τ and the power-delay product *PDP* of the four considered devices. In particular, the three quantities are defined as

$$f_T = \frac{g_m}{2piC_G} \quad (5)$$

$$\tau = \frac{C_G V_{DD}}{I_{on}} \quad (6)$$

$$PDP = V_{DD} I_{on} \tau, \quad (7)$$

where g_m is the transconductance of the device, C_G is the total gate capacitance, V_{DD}=0.8 V is the power supply, and I_{on} is the on-current, defined as the current computed for $V_{\rm GS} = V_{\rm off} + V_{\rm DD}$, where $V_{\rm off}$ is the $V_{\rm GS}$ for which $I_{\rm DS} = I_{\rm off}$. Graphane PMOS show better f_T and smaller *PDP*, which

represents the energy needed to switch the device from ON to OFF state.

II. Conclusion

In conclusion, a multi-scale approach has been adopted in order to assess potential of functionalized graphene as channel material for next-generation high-performance Field-Effect Transistors. To achieve this task, calculations within the GW approximation have been performed in order to compute accurate energy bands and bandgaps, which, in the case of graphone, has been demonstrated to differ by more than 2.7 eV from previous results. Tight-binding Hamiltonians for graphane and graphone have been fitted with DFT results in order to feed a semiclassical model, able to compute transport in the whole Brillouin Zone. Results have shown that graphane and graphone based FETs can provide large current as well as $I_{\rm on}/I_{\rm off}$ ratios, and can represent a promising option for future technology nodes.

Acknowledgment

The work was supported in part by the EC Seventh Framework Program under the Network of Excellence NANOSIL (Contract 216171), the STREP project GRAND (Contract 215752) and the MIUR-PRIN "Modeling and simulation of graphene nanoribbon FETs for high-performance and low-power logic applications" project (Prot. 2008S2CLJ9). S. L. acknowledges financial support from ANR PNANO grant N^0 ANR-06-NANO-053-02 and computer time using HPC resources from GENCI-CCRT/CINES (Grant 2010-085106). M.K. acknowledges financial support from the Swedish Research Council (VR), and the Göran Gustafsson Stiftelse. O.E. acknowledges VR and ERC for support.

References

[1] D. Elias et al., Science, 2009, **323**, 610.
[2] J. Zhou et al, Nano Lett., 2009, **9**, 3867.
[3] S. Koswatta et al., IEEE Trans. Nanotech., 2006, **5**, 386.
[4] J. O. Sofo et al, Phys. Rev. B, 2007, **75**, 153401.
[5] S. Lebègue et al., Phys. Rev. B, 2009, **79**, 245117.
[6] J. Nakamura et al., Appl. Phys. Lett., 2009, **94**, 223107.
[7] M.Z.S. Flores et al., Nanotechnology, 2009, **20**, 465704.
[8] L. Hedin, Phys. Rev., 1965, **139**, A796.
[9] L. Hedin and S. Lundquist, Solid State Physics, 1969, **23**, 1.
[10] G. Kresse and J. Furthmüller, Phys. Rev. B, 1996, **54**, 11169.
[11] G. Kresse and D. Joubert, Phys. Rev. B, 1999, **59**, 1758.
[12] Available online: http://www.itrs.net/Links/2009ITRS/Home2009.htm
[13] P. Michetti, G. Iannaccone, IEEE Trans. El. Dev., 2010, **57** 1616.

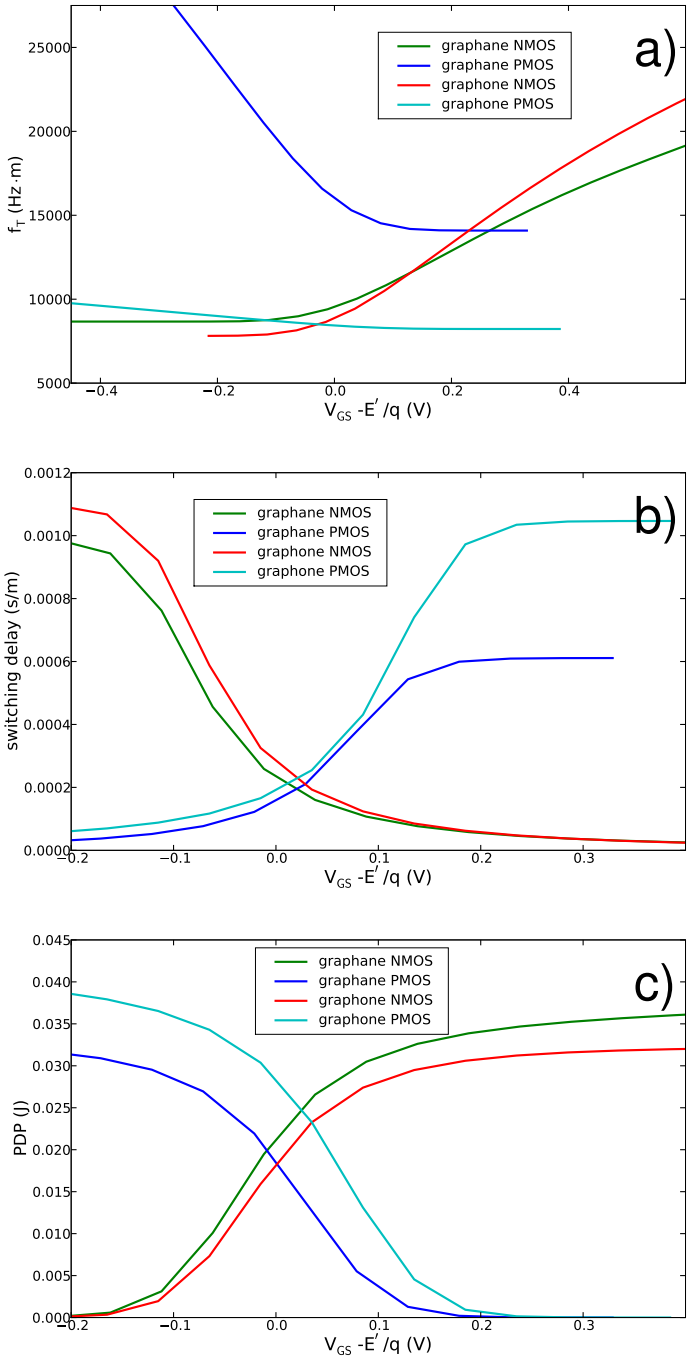

Fig. 5. a) Cut-off frequency, b) switching delay and c) Power-delay product of the 4 considered devices.